Voltage Control of a van der Waals Spin-Filter Magnetic Tunnel Junction

Tiancheng Song,[1] Matisse Wei-Yuan Tu,[2] Caitlin Carnahan,[3] Xinghan Cai,[1] Takashi Taniguchi,[4] Kenji Watanabe,[4] Michael A. McGuire,[5] David H. Cobden,[1] Di Xiao,[3] Wang Yao,[2] Xiaodong Xu[1,6]*

[1]Department of Physics, University of Washington, Seattle, Washington 98195, USA.
[2]Department of Physics and Center of Theoretical and Computational Physics, University of Hong Kong, Hong Kong, China.
[3]Department of Physics, Carnegie Mellon University, Pittsburgh, Pennsylvania 15213, USA.
[4]National Institute for Materials Science, Tsukuba, Ibaraki 305-0044, Japan.
[5]Materials Science and Technology Division, Oak Ridge National Laboratory, Oak Ridge, Tennessee 37831, USA.
[6]Department of Materials Science and Engineering, University of Washington, Seattle, Washington 98195, USA.

*Correspondence to: xuxd@uw.edu

Abstract:

Atomically thin chromium triiodide (CrI_3) has recently been identified as a layered antiferromagnetic insulator, in which adjacent ferromagnetic monolayers are antiferromagnetically coupled. This unusual magnetic structure naturally comprises a series of anti-aligned spin filters which can be utilized to make spin-filter magnetic tunnel junctions with very large tunneling magnetoresistance (TMR). Here we report voltage control of TMR formed by four-layer CrI_3 sandwiched by monolayer graphene contacts in a dual-gated structure. By varying the gate voltages at fixed magnetic field, the device can be switched reversibly between bistable magnetic states with the same net magnetization but drastically different resistance (by a factor of ten or more). In addition, without switching the state, the TMR can be continuously modulated between 17,000% and 57,000%, due to the combination of spin-dependent tunnel barrier with changing carrier distributions in the graphene contacts. Our work demonstrates new kinds of magnetically moderated transistor action and opens up possibilities for voltage-controlled van der Waals spintronic devices.

Keywords: Mangetic tunnel junction, bistable magnetic states, voltage-controlled switching, 2D magnets, van der Waals heterostructure.

Main Text:

Electrical manipulation of magnetism is central to spintronics[1–7]. Voltage-controlled switching between bistable magnetic states can be employed in energy efficient magnetic memory and logic technologies. In this regard, the recently discovered two-dimensional (2D) magnetic insulator chromium triiodide (CrI_3) has several assets as a building block for van der Waals (vdW) spintronics[8–10]. First, the extreme thinness of few-layer CrI_3 enhances the probability that the magnetism will be amenable to electrostatic control[11–16]. Second, the layered antiferromagnetic structure at zero field naturally forms a series of interlayer spin filters, and their relative alignment can be changed by a moderate magnetic field via spin-flip transitions. This unusual property

underpins the recent demonstration of multiple-spin-filter magnetic tunnel junctions (sf-MTJs) that exhibit giant tunneling magnetoresistance (TMR)[17–22].

In multilayer CrI_3, for a given net magnetization there are multiple nearly degenerate magnetic states with different patterns of layer magnetization[17]. Switching between these states reconfigures the interlayer spin filters and thus can change the tunneling resistance. If this switching could be induced by voltage alone it would represent a new kind of magnetic logic. We explore this possibility using a sf-MTJ with four-layer CrI_3 tunnel barrier between monolayer graphene contacts, as shown schematically in Fig. 1a. This sf-MTJ is sandwiched between two hexagonal boron nitride (hBN) flakes with a graphite top gate (held at voltage V_{tg}) and SiO_2/Si substrate used as a bottom gate (at voltage V_{bg}). The monolayer graphene contacts combine a low density of states with high carrier mobility[23,24], allowing much stronger gating effects than using conventional metal electrodes in a vertical junction structure. The tunneling current (I_t) is measured while applying a DC bias voltage (V) to the top graphene contact with the bottom one grounded. All measurements described in the main text, except where specified, were made on the device whose optical image is shown in Fig. 1b (device 1), at a temperature of 2 K.

We first use reflective magnetic circular dichroism (RMCD) to probe the net magnetization[17]. Figure 1c shows the RMCD signal as a function of out-of-plane magnetic field ($\mu_0 H$) swept from negative to positive (orange curve) and vice versa (green curve). It displays typical four-layer CrI_3

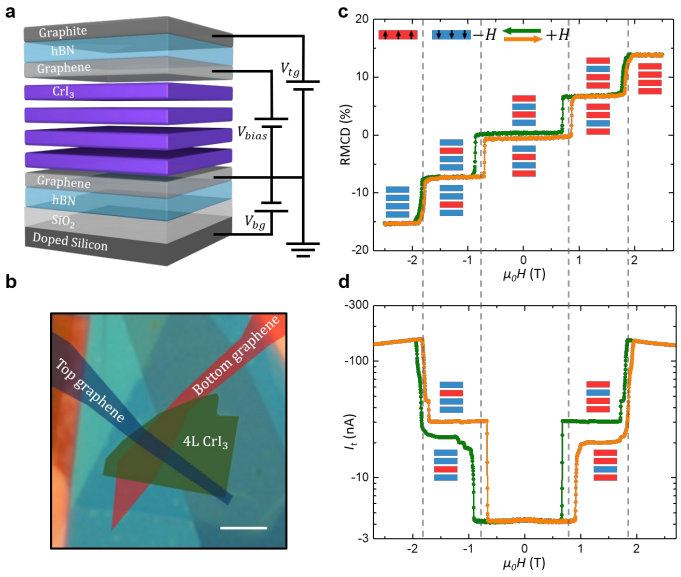

Figure 1 | Magnetic states in four-layer CrI_3 spin-filter magnetic tunnel junction (sf-MTJ). **a**, Schematic of a four-layer CrI_3 sf-MTJ device including two monolayer graphene contacts and top and bottom gates. **b**, False-color optical micrograph of device 1 (scale bar 5 μm). **c**, Reflective magnetic circular dichroism (RMCD) signal as a function of out-of-plane magnetic field ($\mu_0 H$) from device 1. The orange (green) curve corresponds to sweeping the magnetic field up (down). Insets show the corresponding magnetic states. The red and blue blocks denote the out-of-plane magnetization of individual layers pointing up and down, respectively. **d**, Tunneling current (I_t) of the same device at representative bias and gate voltages (V = -240 mV, V_{tg} = 0 V and V_{bg} = 0 V).

behavior[17]. At low fields (<0.7 T) the net magnetization nearly vanishes, corresponding to either of the two fully antiferromagnetic states, ↑↓↑↓ or ↓↑↓↑, as indicated in the figure. The arrows here denote the out-of-plane magnetization from top to bottom layer respectively. The small remnant RCMD signal is caused by a slight asymmetry between the top and bottom layers due to the fabrication process[17]. At high fields (>2 T) the RMCD signal saturates, corresponding to the fully aligned magnetic states, ↑↑↑↑ and ↓↓↓↓. Since the behavior is essentially the same for the opposite field direction, from now on in the discussion we focus on positive magnetic fields.

At intermediate fields (between 0.9 T and 1.7 T) the RMCD signal is about half the saturated value, implying that the net magnetization is half that of the fully aligned state. This is consistent with any of the set of four magnetic states where one layer has the opposite magnetization to the other three, {↑↓↑↑, ↑↑↓↑, ↓↑↑↑, ↑↑↑↓}. Among these, the first two have two antiparallel interfaces while the last two have only one such interface. Since antiparallel interfaces are favored by the antiferromagnetic coupling, the first two should have lower energy. Therefore, we expect the magnetic configuration at intermediate fields to be either ↑↓↑↑ or ↑↑↓↑, these being degenerate and almost indistinguishable if the two internal layers are equivalent.

If a bias is applied either across the junction or between the gates, the RMCD, and thus the net magnetization, does not change, but the electric field can lift the symmetry between ↑↓↑↑ and ↑↑↓↑ and the two states may thus respond differently to the bias, which is expected to yield distinct tunneling magnetoresistance. Figure 1d shows I_t as a function of $\mu_0 H$ with a bias V = -240 mV on the top graphene and both gates grounded. By comparing with Fig. 1c, we see that the lowest and highest current plateaus correspond to the antiferromagnetic and fully aligned magnetic states, respectively. Interestingly, at intermediate magnetic fields where there is only one plateau in the RMCD signal there are two distinct plateaus in the tunneling current. These must correspond to ↑↓↑↑ and ↑↑↓↑, that is, the current is sensitive to which of the internal layers has the minority magnetization. Modeling the system as a set of coupled magnetic quantum wells, we find that ↑↓↑↑ carries the higher tunneling current than ↑↑↓↑ under these conditions, as the former has a transmission resonance closer to the bias window (Supporting Information). We also conclude that

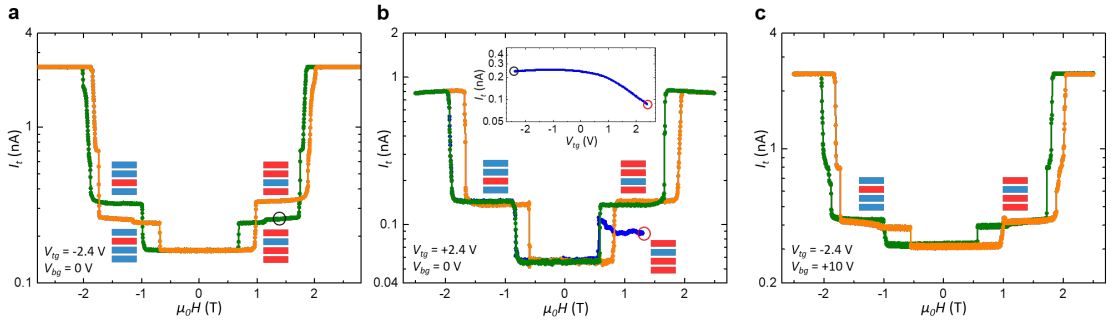

Figure 2 | Electric control of bistable magnetic states. a, **b**, **c**, I_t (V = +80 mV) as a function of $\mu_0 H$ at three representative gate voltages with identified magnetic states as shown in the insets. The orange (green) curve corresponds to sweeping the magnetic field up (down). The inset of **b** shows I_t as sweeping V_{tg} from -2.4 to +2.4 V. The black and red open circles indicate the starting and end points, corresponding to the circles in **a** (initial state) and **b** (final state). Subsequently, $\mu_0 H$ sweeps down and I_t is monitored, as shown by the blue curve in the main panel of **b**.

the system is bistable, remaining in either one of these two magnetic configurations if the field is kept in the intermediate range.

Now we turn to our key finding, which is that switching between the bistable magnetic states can be controlled and induced by gate voltage, and that this affects the tunneling current. Figures 2a-c show I_t (at V = +80 mV) as the field is swept up and down at three selected pairs of gate voltages. At V_{tg} = -2.4 V, V_{bg} = 0 V (Fig. 2a) we see two intermediate-field plateaus, as in Fig. 1d, implying that ↑↓↑↑ and ↑↑↓↑ are similarly stable. However, at V_{tg} = +2.4 V, V_{bg} = 0 V (Fig. 2b, orange and green curves) we see only a higher current plateau, while at V_{tg} = -2.4 V, V_{bg} = +10 V (Fig. 2c) we see only a lower current plateau. This suggests that the latter gate-voltage pairs cause either ↑↑↓↑ or ↑↓↑↑ to be preferred, respectively. Here the small bias V generates tunneling current as a probe of the magnetic states, while V_{tg} plays a dominating role to realize voltage control of the magnetic states. This voltage control of the magnetic states in an additional device is shown in Supporting Information.

To confirm this, we first prepare the system in the low-current state at 1.3 T with the gate voltage pair set at the bistable condition of Fig. 2a, indicated by the black open circle in Fig. 2a. We then sweep V_{tg} from -2.4 to +2.4 V, finishing in the gate voltage condition of Fig. 2b. While doing this we monitor the current, which decreases smoothly (inset to Fig. 2b) to the level at the point indicated by the red open circle in Fig. 2b. When the magnetic field is subsequently swept down (blue curve in Fig. 2b) the current jumps to a lower value below 0.7 T, and thereafter repeated cycling between ±2.5 T simply reproduces the prior behavior with a single intermediate plateau. From these observations we infer that if the system is prepared in the state ↑↓↑↑ at V_{tg} = -2.4 V, then sweeping V_{tg} with the magnetic field fixed is an adiabatic process that maintains it in this state. However, at V_{tg} = +2.4 V this state is only metastable, and it cannot be entered from either fully aligned (highest current) or antiferromagnetic (lowest current) states merely by sweeping the magnetic field.

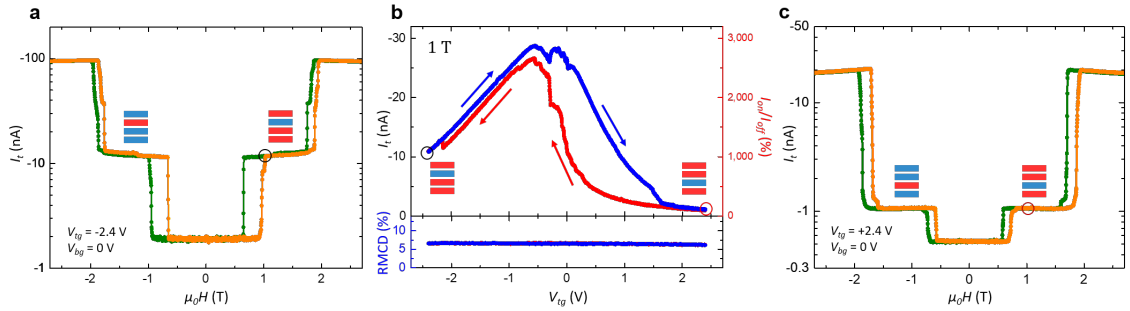

Figure 3 | Reversible voltage switching of the bistable magnetic states. a, **c**, I_t (V = -240 mV) as a function of $\mu_0 H$ at two representative gate voltages with identified magnetic states shown in the insets. **b**, I_t and the extracted magnetoresistance ratio as a function of V_{tg} swept from +2.4 V to -2.4 V (red curve) and back to +2.4 V (blue curve) at fixed $\mu_0 H$ = 1 T. The black and red open circles denote the two ends of the voltage sweep loop, corresponding to the same states circled in **a** and **c**, respectively. The hysteresis curve demonstrates magneto-electric coupling. The bottom panel shows little changes in RMCD during the voltage sweep, consistent with the equal magnetization of the bistable states.

Remarkably, at larger bias voltages it is possible to induce reversible switching between the two magnetic states purely by gate voltage control, while staying at a single fixed magnetic field. Figures 3a and c show the current at V = -240 mV vs magnetic field at V_{tg} = -2.4 V and +2.4 V, respectively, both at V_{bg} = 0 V. The inferred magnetic states are indicated by insets; note that the state that carries the higher current at this negative bias is the one that carried the lower current at the positive bias V = +80 mV (see Fig. 2a). This is self-consistent with bistable states assignment, since the reversal of current flow direction accompanies the reversal of the relative magnitude of I_t between the bistable magnetic states.

If we now fix $\mu_0 H$ = 1 T and sweep V_{tg} up and down between -2.4 V and +2.4 V (Fig. 3b), the current changes repeatably between end values corresponding to ↑↓↑↑ and ↑↑↓↑ (determined from Figs. 3a & c), implying that reproducible switching between these states occurs. Meanwhile, the RMCD signal is almost constant (bottom panel, Fig. 3b), as expected since the two states have the same net magnetization. The general changes in the current with increasing magnitude of V_{tg} is probably associated with doping of the graphene contacts causing a different mismatch of spin or momentum between the contacts. Most interestingly, at intermediate V_{tg} there is pronounced hysteresis in the current, just as expected for a transition between two metastable states, accompanied by small wiggles that are naturally explained by associated domain effects. Within this hysteretic region the current differs between the two states by as much as a factor of ten.

The influence of the gate voltages on the magnetic states can be in principle due to modifications of the anisotropy and interlayer coupling through changes in orbital occupancy and/or electric-field effects modifying the energy splitting of ↑↓↑↑ and ↑↑↓↑. Monte Carlo simulations (Supporting Information) reveal that changing anisotropy alone is not sufficient, and changing interlayer coupling must be included to reproduce the experimental observation.

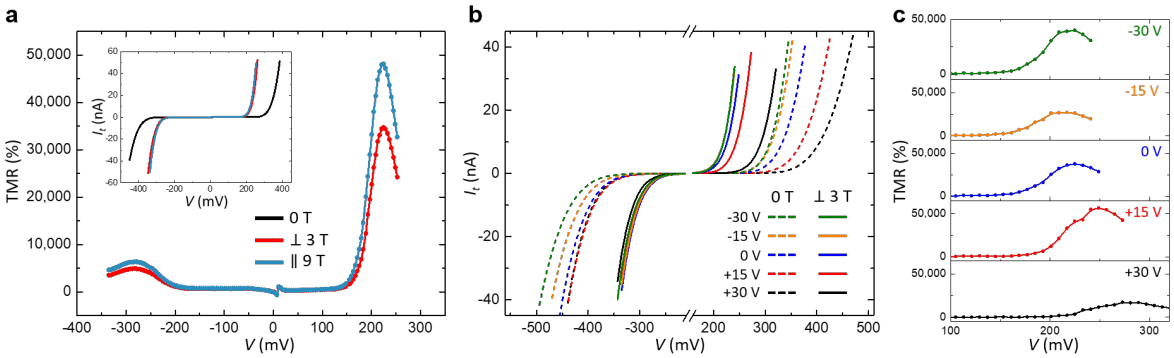

Figure 4 | Gate tunable tunneling magnetoresistance. a, TMR ratio as a function of V derived from the I_t-V data shown in the inset, at V_{bg} = 0 V. **b**, I_t-V curves at five representative gate voltages for layered-antiferromagnetic ground states (dashed curves, at 0 T) and fully aligned magnetic states (solid curves, at 3 T). **c**, TMR ratio as a function of V at a series of V_{bg}.

Finally, we show that direct and dramatic gate-voltage control of the TMR is possible in such devices, irrespective of the switching effect described above. As usual, we define the TMR ratio by $100\% \times (R_{ap}\text{-}R_p)/R_p$, where R_{ap} and R_p are the DC resistances with fully anti-parallel (antiferromagnetic, low-field) and parallel (fully spin-polarized, high-field) layer magnetization measured at a given bias. Figure 4a shows the TMR as a function of bias for device 2 (which has

a single bottom gate), derived from I_t-V curves as shown in the inset for both in-plane and out-of-plane magnetic field at V_{bg} = 0 V. The behavior is similar to that reported previously for ungated devices[17]. The TMR is substantially modified by back gate voltage. Figure 4b shows I_t-V curves for layered-antiferromagnetic states (dashed curves, $\mu_0 H$ = 0 T) and fully aligned states (solid curves, $\mu_0 H$ = 3 T), at V_{bg} values between -30 V and +30 V. There is a consistent shift of the thresholds in these curves towards positive bias as V_{bg} becomes more positive. Figure 4c shows the derived TMR ratio. Its peak value varies from 57,000% to 17,000%. The origin of this behavior is under investigation and beyond the scope of this work, but it may involve a combination of electric field modification of the spin-dependent tunnel barrier (Supporting Information)[25,26], changes of Fermi level and magnetic proximity effects induced by CrI_3 in the monolayer graphene contacts[27,28]. Future experimental work should consider a more complex device geometry that can clarify the effect of carrier concentration and possible magnetic proximity effect of graphene on TMR.

References:

1. Matsukura, F.; Tokura, Y.; Ohno, H. Control of magnetism by electric fields. *Nat. Nanotech.* **2015**, *10*, 209–220.

2. Ohno, H. *et al.* Electric-field control of ferromagnetism. *Nature* **2000**, *408*, 944–946.

3. Chiba, D.; Yamanouchi, M.; Matsukura, F.; Ohno, H. Electrical manipulation of magnetization reversal in a ferromagnetic semiconductor. *Science* **2003**, *301*, 943–945.

4. Weisheit, M. *et al.* Electric field-induced modification of magnetism in thin-film ferromagnets. *Science* **2007**, *315*, 349–351.

5. Maruyama, T. *et al.* Large voltage-induced magnetic anisotropy change in a few atomic layers of iron. *Nat. Nanotech.* **2009**, *4*, 158–161.

6. Wang, W.-G.; Li, M.; Hageman, S.; Chien, C. L. Electric-field-assisted switching in magnetic tunnel junctions. *Nat. Mater.* **2012**, *11*, 64–68.

7. Shiota, Y. *et al.* Induction of coherent magnetization switching in a few atomic layers of FeCo using voltage pulses. *Nat. Mater.* **2011**, *11*, 39–43.

8. Huang, B. *et al.* Layer-dependent ferromagnetism in a van der Waals crystal down to the monolayer limit. *Nature* **2017**, *546*, 270–273.

9. Seyler, K. L. *et al.* Ligand-field helical luminescence in a 2D ferromagnetic insulator. *Nat. Phys.* **2018**, *14*, 277–281.

10. Huang, B. *et al.* Electrical control of 2D magnetism in bilayer CrI_3. *Nat. Nanotech.* **2018**, *13*, 544–548.

11. Zhong, D. *et al.* Van der Waals engineering of ferromagnetic semiconductor heterostructures for spin and valleytronics. *Sci. Adv.* ***2017***, *3*, e1603113.

12. Geim, A. K. and Grigorieva, I. V. Van der Waals heterostructures. *Nature* **2013**, *499*, 419–425.

13. Novoselov, K. S.; Mishchenko, A.; Carvalho, A.; Castro Neto, A. H. 2D materials and van der Waals heterostructures. *Science* **2016**, *353*, aac9439.

14. Jiang, S.; Shan, J.; Mak, K. F. Electric-field switching of two-dimensional van der Waals magnets. *Nat. Mater.* **2018**, *17*, 406–410.

15. Jiang, S.; Li, L.; Wang, Z.; Mak, K. F.; Shan, J. Controlling magnetism in 2D CrI_3 by electrostatic doping. *Nat. Nanotech.* **2018**, *13*, 549–553.

16. Sivadas, N.; Okamoto, S.; Xiao, D. Gate-controllable magneto-optic Kerr effect in layered collinear antiferromagnets. *Phys. Rev. Lett.* **2016**, *117*, 267203.

17. Song, T. *et al.* Giant tunneling magnetoresistance in spin-filter van der Waals heterostructures. *Science* **2018**, *360*, 1214–1218.

18. Klein, D. R. *et al.* Probing magnetism in 2D van der Waals crystalline insulators via electron tunneling. *Science* **2018**, *360*, 1218–1222.

19. Wang, Z. *et al.* Very large tunneling magnetoresistance in layered magnetic semiconductor CrI_3. *Nat. Commun.* **2018**, *9*, 2516.

20. Kim, H. H. *et al.* One million percent tunnel magnetoresistance in a magnetic van der Waals heterostructure. *Nano Lett.* **2018**, *18*, 4885-4890.

21. Worledge, D. C. and Geballe, T. H. Magnetoresistive double spin filter tunnel junction. *J. Appl. Phys.* **2000**, *88*, 5277–5279.

22. Miao, G.-X.; Müller, M.; Moodera, J. S. Magnetoresistance in double spin filter tunnel junctions with nonmagnetic electrodes and its unconventional bias dependence. *Phys. Rev. Lett.* **2009**, *102*, 076601.

23. Novoselov, K. S. *et al.* Two-dimensional gas of massless Dirac fermions in graphene. *Nature* **2005**, *438*, 197–200.

24. Zhang, Y.; Tan, Y.-W.; Stormer, H. L.; Kim, P. Experimental observation of the quantum Hall effect and Berry's phase in graphene. *Nature* **2005**, *438*, 201–204.

25. Lezlinger, M. and Snow, E. H. Fowler-Nordheim tunneling into thermally grown SiO_2. *J. Appl. Phys.* **1969**, *40*, 278–283.

26. Britnell, L. *et al.* Field-effect tunneling transistor based on vertical graphene heterostructures. *Science* **2012**, *335*, 947–950.

27. Greenaway, M. T. *et al.* Resonant tunnelling between the chiral Landau states of twisted graphene lattices. *Nat. Phys.* **2015**, *11*, 1057–1062.

28. Wei, P. *et al.* Strong interfacial exchange field in the graphene/EuS heterostructure. *Nat. Mater.* **2016**, *15*, 711–716.

29. Blake, P. *et al.* Making graphene visible. *Appl. Phys. Lett.* **2007**, *91*, 063124.

30. Zomer, P. J.; Guimarães, M. H. D.; Brant, J. C.; Tombros, N.; van Wees, B. J. Fast pick up technique for high quality heterostructures of bilayer graphene and hexagonal boron nitride. *Appl. Phys. Lett.* **2014**, *105*, 013101.

31. Sato, K. Measurement of magneto-optical Kerr effect using piezo-birefringent modulator. *Jpn. J. Appl. Phys.* **1981**, *20*, 2403–2409.

Methods:

Device fabrication

CrI_3 crystals were mechanically exfoliated onto 90 nm SiO_2/Si substrates in a nitrogen glove box with water and oxygen concentration less than 0.5 ppm. The four-layer CrI_3 flakes were identified by their optical contrast relative to the substrate using the established optical contrast models of CrI_3[8,29]. The monolayer graphene, graphite and 5-30 nm hBN flakes were exfoliated onto either 285 nm or 90 nm SiO_2/Si substrates and examined by optical and atomic force microscopy under ambient conditions. Only atomically clean and smooth flakes were identified and used. Metallic V/Au (7/70 nm) electrodes were deposited onto the bottom hBN flakes and substrates using electron beam evaporation before a standard electron beam lithography with a bilayer resist (A4 495 and A4 950 poly (methyl methacrylate (PMMA))). The van der Waals stacking was performed in the glove box using a polymer-based dry transfer technique[30]. The flakes were picked up sequentially: top gate graphite, top hBN, top monolayer graphene contact, four-layer CrI_3, bottom monolayer graphene contact. The resulting stacks were then transferred and released on top of the bottom hBN with pre-patterned electrodes. In the complete heterostructure, the CrI_3 flake is fully encapsulated, and the top/bottom monolayer graphene and the top gate graphite flakes are connected to the pre-patterned electrodes.

Electrical measurement

The electrical measurements were performed in a PPMS DynaCool cryostat (Quantum Design, Inc.) with a base temperature of 1.7 K. The four-layer CrI_3 sf-MTJ devices were mounted in a Horizontal Rotator probe, which allows applying out-of-plane or in-plane magnetic field up to 9 T. Figure 1a shows the schematic of four-layer CrI_3 sf-MTJs. The DC bias voltage (V) is applied to the top monolayer graphene contact with the bottom monolayer graphene contact grounded. The top and bottom gate voltages (V_{tg} and V_{bg}) are applied to the top gate graphite and bottom doped Si substrate, respectively. The resulting tunneling current (I_t) is amplified and measured by a current preamplifier (DL Instruments; Model 1211).

Reflective magnetic circular dichroism measurement

The reflective magnetic circular dichroism (RMCD) measurements were performed in an attocube closed-cycle cryostat (attoDRY 2100) with a base temperature of 1.55 K and up to 9 T magnetic field in the out-of-plane direction. A power-stabilized 632.8 nm HeNe laser was used to probe the device at normal incidence with a fixed power of 1 μW. The AC lock-in measurement technique used to measure the RMCD signal follows closely to the previous magneto-optical Kerr effect (MOKE) and RMCD measurements of the magnetic order in atomically-thin CrI_3[8,17,31].

Acknowledgements: We thank Yongtao Cui for insightful discussion. Funding: Work at the University of Washington was mainly supported by the Department of Energy, Basic Energy Sciences, Materials Sciences and Engineering Division (DE-SC0018171). Device fabrication and part of transport measurements are supported by NSF-DMR-1708419, NSF MRSEC 1719797, and UW Innovation Award. D.H.C. is supported by DE-SC0002197. Work at CMU is supported by DOE BES DE-SC0012509. Work at HKU is supported by the Croucher Foundation (Croucher Innovation Award), RGC of HKSAR (17303518P). Work at ORNL (M.A.M.) was supported by the US Department of Energy, Office of Science, Basic Energy Sciences, Materials Sciences and Engineering Division. K.W. and T.T. acknowledge support from the Elemental Strategy Initiative

conducted by the MEXT, Japan and JSPS KAKENHI Grant Numbers JP15K21722. D.X. acknowledges the support of a Cottrell Scholar Award. X.X. acknowledges the support from the State of Washington funded Clean Energy Institute and from the Boeing Distinguished Professorship in Physics.

Author Contributions: X.X. and T.S. conceived the project. T.S. fabricated the devices, performed the experiments, and analyzed the data, assisted by X.C., supervised by X.X., D.X., W.Y., and D.H.C.. M.W.-Y.T. and W.Y. modeled the tunneling current. C.C. and D.X. performed the Monte Carlo simulation. M.A.M. provided and characterized bulk CrI_3 crystals. T.T. and K.W. provided and characterized bulk hBN crystals. T.S., X.X., D.H.C., D.X., and W.Y. wrote the manuscript with input from all authors.

Competing Financial Interests: The authors declare no competing financial interests.

Data Availability: The data that support the findings of this study are available from the corresponding author upon reasonable request.